The MPU RX-4 Project: Design, Electronics, and Software Development of a Geofence Protection System for a Fixed-Wing VTOL UAV

Konstantinos A. Tsintotas, *Senior Member, IEEE*, Loukas Bampis, Anastasios Taitzoglou, Ioannis Kansizoglou, Pavlos Kaparos, Chris Bliamis, Kyros Yakinthos, and Antonios Gasteratos, *Senior Member, IEEE*

***Abstract*— Unmanned aerial vehicles (UAVs) are at the forefront of this century's technological shift, becoming ubiquitous in research and market areas. However, as a UAV navigates autonomously, there are unanticipated occasions, e.g., collisions with dynamic obstacles or loss of data provided by the global navigation satellite system (GNSS), where the aircraft has to change its mission plans. In particular, to be protected from possible accidents, the platform's geofence protection system should adjust the trajectory appropriately when obstacles are detected and select the proper ground surface when emergency landing is prompted. As these processes require fast reaction times, utilizing low latency sensors and algorithms is necessary. This article proposes a complete and low-complexity geofence protection system for recognizing moving objects and assessing the ground surface's suitability using onboard sensing and processing modules. The proposed system is implemented on a novel fixed-wing UAV, designated as MPU RX-4, which features an unconventional flying wing layout and vertical take-off and landing (VTOL) capabilities. Our system is based on a forward-facing laser imaging, detection, and ranging (LIDAR) sensor and three downward-facing laser rangefinders. We take advantage of the high-precision distance measurements and operational speed to identify moving obstacles using the LIDAR module, while the ground's slope and the existence of any obstacle therein are computed through the rangefinders. First, the article describes the UAV design procedure and its aerodynamic performance characteristics, which allowed us to evaluate our approach on a testbed aircraft. Then, the evaluation protocol shows that our system can perform robustly and under real-time constraints reaching an overall latency of only 165.5 ms, sufficient for reliable detection and avoidance of moving obstacles.**

***Index Terms*— Geofence protection system, unmanned aerial vehicle (UAV), vertical take-off and landing (VTOL), visual-based navigation.**

I. Introduction

IN ROBOTICS literature, unmanned aerial vehicles (UAVs) are usually called multicopter platforms or microaerial vehicles (MAVs) [1]. Due to the market's demands for various military, commercial, and industrial applications, these systems have become widely popular in the research community [2]. However, their growth is mainly owed to the significant technological advances in machine autonomy [3], [4]. Representative examples include traffic and farming surveillance [5], [6], asset monitoring [7], wildfire detection [8], [9], investigation of hazardous environments [10], [11], product delivery [12], [13], structure inspection (such as power cables, dam walls, vessels, and bridges) [14], [15], [16], [17], [18], and search-and-rescue missions [19], [20].

The main components for achieving such autonomous tasks are take-off [21], trajectory tracking [22], [23], and precise landing [24]. Nevertheless, primarily based on a global navigation satellite system (GNSS) receiver [25], trajectory tracking and landing are the most critical among the abovementioned ones. Unfortunately, several accidents have been reported over the last years due to obstacles in the aircraft's path and the selection of unsuitable ground surfaces during landing [26]. Moreover, methods based on GNSS are susceptible to interference [27], which increases the accident rate when navigation and landing are performed in complex environments. Yet, the difficulty in both situations is related to the task of the flight controller to generate a proper trajectory while minimizing power consumption and providing robustness in the face of dynamic conditions, e.g., moving obstacles [28], [29], [30], sudden wind gusts and rotor downwash [31], moving landing platforms [32], or unsuitable landing surfaces [33], such as rocky surroundings or high slope [34]. However, today's UAVs are still restricted by their onboard processing power, which

Manuscript received 5 July 2022; revised 15 September 2022; accepted 14 November 2022. Date of publication 28 November 2022; date of current version 10 January 2023. This work was supported in part by the European Regional Development Fund, Partnership Agreement for the Development Framework (2014–2020) within the project "MPU-Multirole Portable UAS" and in part by the Greece and European Union in the framework of OPERATIONAL PROGRAM: "Competitiveness, Entrepreneurship and Innovation 2014-2020 (EPAnEK)," Nationwide Action: "Research - Create - Innovate" under Project T1EDK-00737. The Associate Editor coordinating the review process was Branislav Djokic. *(Corresponding author: Konstantinos A. Tsintotas.)*

Konstantinos A. Tsintotas, Anastasios Taitzoglou, Ioannis Kansizoglou, and Antonios Gasteratos are with the Department of Production and Management Engineering, Democritus University of Thrace, 67132 Xanthi, Greece (e-mail: ktsintot@pme.duth.gr; ataitzog@pme.duth.gr; ikansizo@pme.duth.gr; agaster@pme.duth.gr).

Loukas Bampis is with the Department of Electrical and Computer Engineering, Democritus University of Thrace, 67100 Xanthi, Greece (e-mail: lbampis@ee.duth.gr).

Pavlos Kaparos, Chris Bliamis, and Kyros Yakinthos are with the Department of Mechanical Engineering, Aristotle University of Thessaloniki, 54124 Thessaloniki, Greece (e-mail: pkaparos@meng.auth.gr; bliamis@meng.auth.gr; kyak@meng.auth.gr).

Digital Object Identifier 10.1109/TIM.2022.3225020

is insufficient for reacting promptly in such cases. Due to this fact, frameworks that evaluate the safety level of the aircrafts' trajectory planning and landing procedures are becoming a popular research topic [35], [36], [37].

Aiming to autonomously navigate on a large scale, vehicles need a geofence protection system capable of working with low latency sensors and algorithms [38]. Over the past decade [39], much research has been conducted based on visual sensory information [40], [41], [42], [43], [44]. Due to their low-cost [45], [46] and low-interference characteristics [47], [48], [49], [50], vision-based systems have been proven reliable for different vehicle types [51], [52], [53], including vertical take-off and landing (VTOL) platforms [54], [55], [56]. However, as most image-based computer vision algorithms for geofencing are prone to errors [57], [58], researchers focus on robust measurements provided by laser scanners [59], such as laser imaging, detection, and ranging (LIDAR) sensors [60], [61], [62], [63]. Yet, failures and faults in sensor measurements, expressed as anomalies in the flight data, are recognized through anomaly detection methods [64], [65], [66], [67].

Since a geofence protection system holds a vital role in the mission's integrity when developing a fully autonomous UAV, in this article, we propose a lightweight and low-complexity pipeline to detect and avoid obstacles in the aircraft's path, as well as a landing method to compute the surface's slope together with potential obstacles therein under real-time constraints [68]. This way, we address the challenge of protecting a UAV from possible accidents through a framework that uses only onboard sensing and computation [69]. Our pipeline adopts the measurements given by a forward-facing LIDAR for interpreting and evaluating the aircraft's view, while three downward-facing laser range finders are responsible for providing the ground surface's suitability. More specifically, exploiting the temporal information in the event stream, we distinguish objects between static and dynamic ones, while an efficient strategy issues appropriate control commands to avoid potential obstacles. Similarly, a low-complexity algorithm detects protruding objects, e.g., rocks or tree trunks, based on the repetitive measurements given by the downward-facing sensors. To assess our approaches, a prototype testbed hybrid fixed-wing VTOL UAV, dubbed MPU RX-4 [70], [71], was developed and evaluated. Our extensive experimental evaluation protocol is provided for several challenging cases. The main contributions of the article at hand are as follows.

1) First, a complete geofence protection system for evaluating moving objects during navigation and the ground surface's suitability for emergency landing is introduced. This system is based on two types of laser sensors:
   a) a solid LIDAR sensor, i.e., without moving parts, which is used for the recognition of obstacles in the UAV trajectory;
   b) three range finders for the recognition of landing surface suitability to make it possible for the entire framework to run in real time.
2) Second, a low-complexity obstacle detection pipeline based on the measurements provided by the LIDAR is proposed, capable of achieving real-time performance on an embedded Intel Edison computer. We consider the magnitude and the direction of the obstacle's velocity to decide which path to evade, and we introduce a decaying factor to account for dynamic obstacles.
3) Third, the MPU RX-4 platform's detailed design and implementation are also presented, featuring an innovative and efficient VTOL propulsion system, together with its computational fluid dynamics (CFD)-aided performance.
4) Fourth, a qualitative and quantitative evaluation protocol was developed and presented, aiming to provide the results of the proposed geofence protection system regarding on the detection accuracy and computational complexity.

The remainder of this work is organized as follows. Section II provides an extensive description of the MPU RX-4 platform's design and Section III presents its CFD modeling. Next, Section IV clarifies the proposed geofence protection mechanism, while the system's experimental evaluation is presented in Section V. Finally, our conclusions are outlined in Section VI.

A. VTOL—UAVs Foundation

Today's available UAVs are categorized based on their external dimensions, viz., the gross take-off weight (GTOW) or the means of lift generation. Concerning the latest, different platforms are classified as fixed-wing or multirotor. Several exclusive advantages and inherent limitations exist for each case. More specifically, fixed-wing UAVs exhibit reduced aerodynamic drag, smaller thrust-to-weight requirements, and improved aerodynamic design. However, on the one hand, these attributes improve aerodynamic performance characteristics, such as higher endurance, flight range, and payload capacity. On the other hand, their main disadvantages refer to the need for a runway or launch-and-recovery system (i.e., catapult and recovery net) and their inability to operate in confined environments at very low speeds (stall velocity limitation) [72]. Contrariwise, multirotor UAVs can take-off and land at a broader range of areas, while through their unique hovering capability, they can be adopted for several complex missions. Nevertheless, they require a higher thrust-to-weight ratio while presenting increased aerodynamic drag due to several exposed parts. Furthermore, the continuous operation of their motors results in significantly higher power consumption. Hence, their overall endurance, range, and maximum speed are severely limited [73].

In recent years, hybrid designs have come to the foreground, incorporating the benefits of both configurations while minimizing their disadvantages. These UAVs (e.g., VTOL, hover, fixed-wing cruise) can operate at a wider flight envelope and, simultaneously, are suitable for a more extensive range of missions. Based on how their take-off and landing are performed [74], they are further categorized into tailsitter, tilt-rotor, and tilt-wing or dual-system. Usually, designers select dual-system configurations, where the VTOL and fixed-wing flight segments are entirely separated, i.e., each uses a different

propulsion system. These VTOL UAVs, such as the Latitude Engineering's HQ-60 and the AeroVironment's T-20 [75], have been operational for many years. Their primary advantage lies in their relative design and manufacturing simplicity, which is highly attractive to UAV designers. At the same time, further research is still conducted in their domain, as indicated by Dündar et al. [73] and Tyan et al. [76]. However, dual-system configurations exhibit poorer aerodynamic behavior. This is owed to two main reasons. First, the presence of booms increases the UAV's wetted area, and thus, the friction-related drag. On the other hand, their exposed motors and propellers are a source of additional losses due to vortexes and windmilling drag. Next, the second most popular VTOL system is the tilt-rotor or tilt-wing, which both share many similarities in flight mechanics. Their distinction is based on the overall UAV's geometry, the sizing, and the design of the tilting mechanisms. Most notably, significant corporations and research agencies are developing such UAVs, for instance, the IAI with the tilt-rotor Panther UAV [77], and NASA and JAXA with the tilt-wing GL-10 [75] and QUX-02 [72], respectively. These designs avoid the dual systems' issues but are more complex to design and implement, requiring additional regular maintenance of the rotating parts. Additionally, this type of VTOL increases the UAV's GTOW, which in some cases can result in poorer aerodynamic characteristics compared to a simple dual-system design. Finally, tailsitter systems can feature the minimum number of required motors (i.e., two) for both VTOL and fixed-wing flight segments, which do not need tilt during the transition. This can provide a unique advantage in terms of GTOW and design complexity. However, tailsitter systems suffer from two main drawbacks. First, a highly advanced and complex autopilot system is required to perform VTOL and transition under wind conditions with only two motors. Moreover, tailsitter UAVs are limited to small GTOWs, since the motor sizing is directly related to it, and large GTOW values could result in front-heavy and highly unstable designs. The most successful tailsitter UAV that is operational for mapping and monitoring applications is the WingtraOne [78].

Despite the usually increased weight requirements of fixed-wing VTOL UAVs, they still operate at a wider flight envelope than their conventional fixed-wing counterparts due to additional motors, batteries, and auxiliary systems. Therefore, based on the statement above, the proposed MPU-RX4 follows a hybrid configuration that exploits the advantages of performing under different environment cases while preserving high efficiency. Specifically, the MPU RX-4 features a flying wing layout while a hybrid tilt-wing/dual system performs its propulsion. In addition, two main motors are mounted on the canards, which can be rotated independently of one another, and are utilized during VTOL and fixed-wing flight. The UAV performs VTOL as a tricopter configuration, with a third fixed motor mounted on the rear side and which operates only during VTOL. During the fixed-wing flight, the third motor is concealed within the UAV's main body by dedicated hatches [79], thus minimizing any potential drag increase from additional exposure to the flow parts.

B. Problem Statement

To maintain any autonomous UAV intact during a mission, the perception system must identify and avoid moving obstacles as quickly as possible since a collision can damage the environment, cause severe hardware failures, or even harm humans [80]. Similarly, when an emergency landing is required due to unforeseen scenarios (such as low remaining power or loss of communication between the UAV and the ground station), the geofence protection mechanism needs to recognize the surface conditions where the platform should land. However, as the temporal latency between perception and action plays a crucial role in both cases [81], the computational complexity of the algorithms and the type of sensory readings need to be restrained [82], [83]. The existing literature on obstacle avoidance relies heavily on conventional cameras (either in a monocular [84], [85], [86], [87] or a stereo configuration [88], [89], [90], [91]), as well as depth cameras [92], [93], [94]. Still, in most cases, the obstacles are assumed to be either static or quasi-static, i.e., following a slow relative motion with respect to the vehicle's frame of reference [95]. Recently, event cameras, which are bio-inspired sensors with reaction times of microseconds, have attracted the interest of the robotics community [96]. Obstacle detection is among the applications with the highest potential, while their applicability for collision detection [97] and object tracking [98], [99] is also explored. However, standard vision algorithms cannot be applied to event cameras because their output is not images but a stream of asynchronous events that encode per-pixel intensity changes [30]. Therefore, the most appropriate solution for such time-critical applications still relies on low-latency sensors, such as lasers [100], [101], which have reaction times of microseconds.

Additionally, as UAVs have reduced payload capabilities, which puts a hardbound on the sensing and computing resources they can carry, laser ranger finders [68] or ultrasonic [34] sensors are selected to measure the distance from the ground and recognize its suitability for landing. Thus, MPU RX-4, a platform capable of landing vertically on its underbelly, is equipped with an LIDAR and three laser range finders. Furthermore, another set of sensors, viz., a GNSS receiver and an inertial measurement unit (IMU), is also mounted on its platform to perform autonomous navigation. The LIDAR is used to perceive the environment's surroundings and avoid collision with moving or static obstacles during the flight, while the laser rangefinders and IMU are considered for the aircraft's autonomous landing. These facing downward are employed for measuring the aircraft's altitude above the ground. More specifically, one long-range rangefinder is adopted for landing and retaining a minimum safety distance from the ground, while the rest are low range and utilized solely for landing. Unlike the other works in the field [102], we focus on protecting the whole system's integrity, and for this reason, we present the design of the aircraft on top of which we developed our novel algorithms. Finally, a set of experiments are conducted to evaluate the optimal tradeoff between the detection speed and accuracy of the obstacles in the aircraft's view and the surface's suitability in an emergency landing.

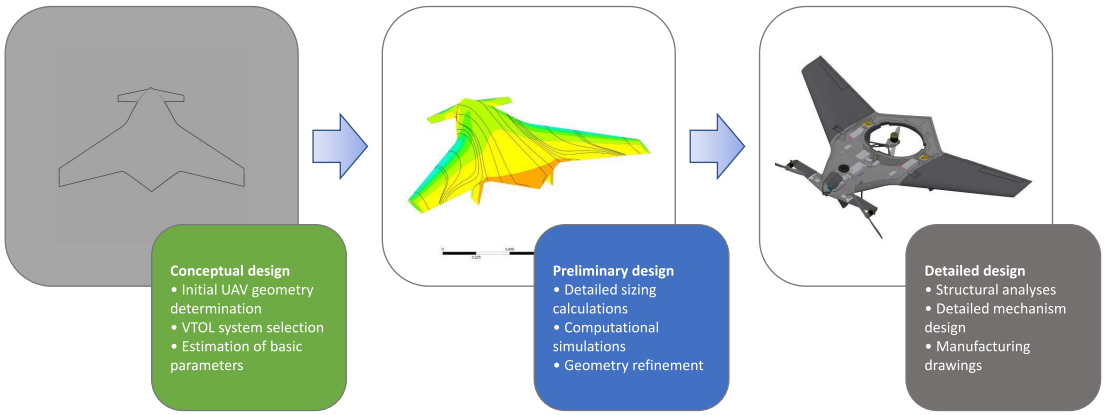

Fig. 1. Phases followed to design the proposed VTOL UAV, dubbed as MPU RX-4. Like most aerial vehicles, the design process consists of conceptual, preliminary, and detailed design phases. During the first stage, the initial concept was selected. Next, a more detailed design was calculated in the preliminary design, while the final platform was concluded in the last stage.

II. MPU RX-4 Framework

Section II presents the MPU RX-4 implementation. A detailed description of its design characteristics is provided in [79]. However, in order for this article to be self-contained, we first summarize the following procedures: conceptual, preliminary, and detailed design (see Fig. 1). Subsequently, we present the electronics' deployment, which allows the proposed geofence system to perceive the environment.

A. Fixed-Wing VTOL UAV Design

As the utilized hybrid VTOL fixed-wing UAV is a custom-made platform constructed and assembled from scratch, the initial geometry and basic parameters of the UAV were determined in the conceptual phase. Then, two distinct VTOL capability configurations were examined based on traditional analytical presizing methods, i.e., low fidelity and semi-empirical correlations, and some initial CFD modeling [70]. During preliminary design, detailed sizing calculations were performed for each UAV component [71], [79]. At the same time, regarding the structural point of view, we investigated the design of the mechanisms responsible for the transition from a vertical orientation to a horizontal one. These actions resulted in a refined weight, while several limitations were raised concerning the MPU RX-4 sizing and its component placement. Next, different modifications were performed to the aircraft's external geometry regarding the canards' sizing and the triple-fin landing system. In addition, the aerodynamic and stability performance was further examined at this phase. More specifically, the sizing of 11 control surfaces and the detailed analyses through CFD modeling concluded the impact of geometry alteration and weight increase. The stability performance of the UAV was modeled with stability and control derivatives, which are computed following the methodology of Roskam [103], though specifically modified for lightweight tailless UAVs [71]. The main challenge of the MPU RX-4 in terms of stability and controllability lies mostly in its lack of empennage (i.e., absence of vertical and horizontal stabilizers) and directional control surfaces. Finally, the vehicle's external geometry, structural analyses, and final manufacturing drawings were considered within the detailed design. The latter included every necessary information related to the type and number of carbon fiber layers constituting the overall composite structure of the UAV. The resulting configuration of the MPU RX-4 is illustrated in Fig. 2. As shown, its basic external dimensions are given for both the take-off and landing processes as well as during navigation (fixed-wing with closed segments).

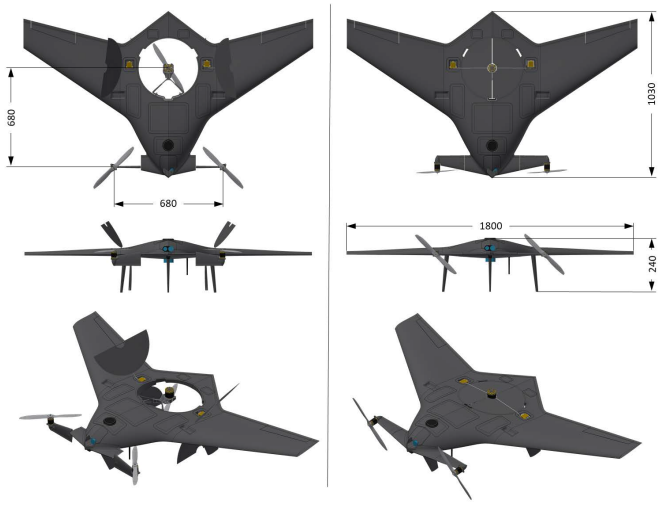

Fig. 2. MPU RX-4 UAV configuration during the VTOL (left) and fixed-wing segments (right).

B. Sensor Payload and Layout

The environment perception sensors are necessary to ensure the aircraft's integrity during flight missions. This way, the forward-facing LIDAR sensor was mounted to the aircraft's beak in the presented aircraft, while the three downward-facing laser rangefinders were mounted in the vehicle's belly (see Fig. 3). More specifically, the LIDAR sensor, a LeddarTech LeddarVu8,[1] was selected to be of wide range and

[1] https://tinyurl.com/leddar-vu8

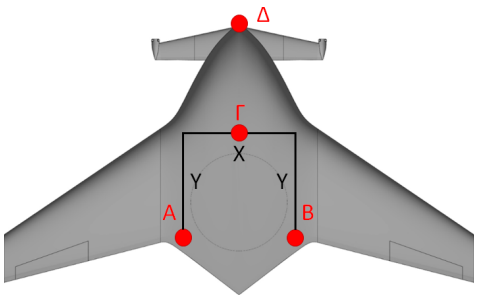

Fig. 3. Overview of the sensors' position in the proposed VTOL aircraft. Points A and B, at the back of the aircraft, denote the two low-range laser rangerfinders, while point Γ is the long-range distance sensor located at the center of the vehicle. The last point Δ denotes the LIDAR sensor's position, which mounted on the vehicle's beak.

amplitude, aiming to monitor a large-scale environment and detect objects that may intervene with the aircraft's trajectory.

Among the three downward-facing sensors, the long-range rangefinder, an SF11/C,[2] is responsible for retaining a safe distance between the UAV and the ground, while the rest, two TeraRanger One,[3], are low-range and are used only during surface suitability evaluation. Regarding their spatial arrangement, the long-range sensor is located at the UAV's center, while the low-range ones are at the back of the aircraft.

Moreover, MPU RX-4 is equipped with a Hex Cube Black[4] flight controller (previously known as Pixhawk 2.1) flashed with PX4[5] software, a commercial autopilot suite that provides internal access to the flight controller and its parameters. However, since the processing of the above measurements needs to operate in real-time during navigation, an Intel Edison processor is also mounted internally as a companion computer to the flight controller board, aiming to increase the system's computational capabilities. The proposed geofence protection scheme is executed on the hosted companion computer, flashed with a Linux operating system. Concerning the data provided by the three downward-facing laser rangefinders to the controller and subsequently to the companion computer, the inter-integrated circuit (I^2C) and MAVs communication protocol (MAVLink[6]) are used. In contrast, the LIDAR measurements are provided to the flight controller through the serial protocol. This way, the Hex Cube Black is utilized as an off-the-shelf solution for reading the acquired distance measurements. In Fig. 4, the proposed flight system is presented, while the overall specifications are displayed in Table I.

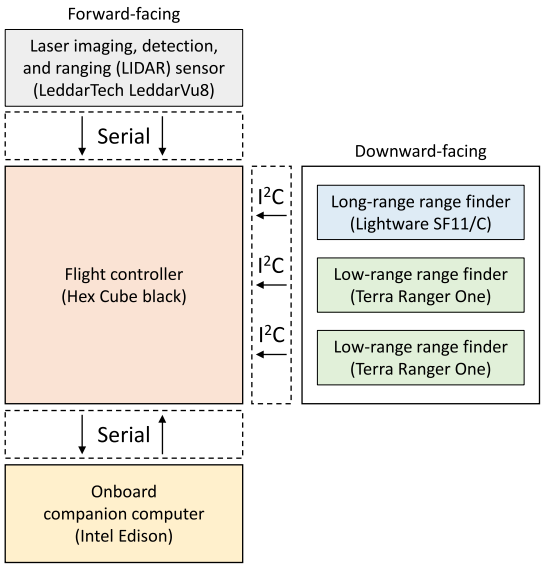

Fig. 4. Overview of the proposed geofence protection system. The flight controller communicates with the forward-facing LIDAR sensor and the internal companion computer through the serial protocol, while the downward-facing rangefinders use the I^2C protocol.

TABLE I
MPU RX-4 SPECIFICATIONS

	Specifications
Type	Vertical take-off and landing (VTOL)
Dimensions (W × H)	1800mm × 1030mm
Maximum take-off weight	7.5 Kg
Flight controller	Hex Cube Black (known as Pixhawk 2.1)
Onboard computer	Intel Edison (Atom 2-Core 500 MHz CPU)
Laser range-finder (1)	TeraRanger One (up to 14 meters)
Laser range-finder (2)	TeraRanger One (up to 14 meters)
Laser range-finder (3)	LightWare SF11/C (up to 120 meters)

III. MPU RX-4 CFD MODELING

As previously stated, during the design process of a UAV, high-fidelity CFD computations are necessary for the accurate prediction of the aerodynamic characteristics and the estimation of the UAV's flight performance subsequently. Therefore, concerning the CFD modeling of MPU RX-4, the steady-state incompressible Reynolds Averaged Navier–Stokes (RANS) equations were solved, and the one equation eddy viscosity turbulence model of Spalart and Allmaras was used for their closure [104]. The Spalart–Allmaras is a widely used turbulence model in aeronautical applications, ranging from commercial airliners to mini fixed-wing UAVs [105], [106]. Since CFD modeling required significant computational resources, the geometry used in the modeling is a simplified version of the one presented in Fig. 2, with the nonessential details being omitted without loss in aerodynamic accuracy. The contribution of these omitted details is relatively small and is calculated through the analytical methods presented by Roskam [103], and thus are deemed nonessential. The results of CFD modeling were also compared against those obtained from the previously mentioned analytical methods, which are widely used in the aircraft design process, and were in very close agreement. The necessary computational meshes were unstructured and were generated with the BETA ANSA preprocessing software (v21.0.1). Each one presents a structured-like region near the solid wall surfaces of the UAV, with 25 cells in the normal to the wall direction, to accurately capture the boundary layer development. The total number of

[2]https://tinyurl.com/sf11-c-120m
[3]https://tinyurl.com/teraranger1
[4]https://tinyurl.com/HexCubeBlack
[5]https://tinyurl.com/px4io
[6]https://tinyurl.com/mavlinkio

computational cells for the mesh used is around 12 million, resulting from grid independence studies previously performed at cruise conditions.

The UAV is designed to operate at altitudes less than 400 ft, complying with Greek National regulations concerning UAV flights. Hence the air properties for the CFD modeling correspond to that altitude, based on the U.S. Standard Atmosphere model. As for the boundary conditions related to turbulence parameters, only the eddy viscosity ratio must be defined and is set equal to 0.21 [107].

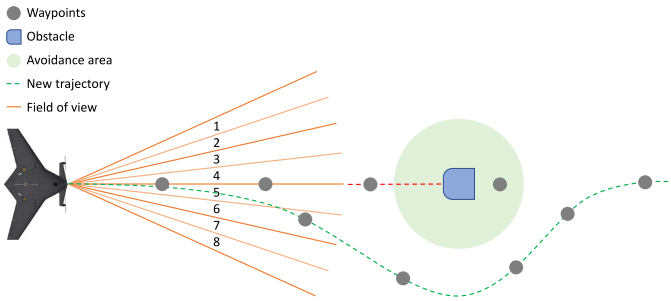

Fig. 5. Obstacle avoidance during navigation.

IV. MPU RX-4 Geofence Protection System

This section presents the proposed methods for the UAV's onboard geofence protection system. Our techniques for obstacle avoidance and landing surface evaluation are based on the selected perception sensors. In particular, the primary function of the long-range rangefinder is to identify changes over the ground's elevation to adjust the flight altitude of the UAV during its mission. If the measured distance between the vehicle and the ground surfaces falls below a threshold, i.e., 30 m, adjustments are performed lifting the UAV at a safer position. Its secondary function lies in its cooperation with the rest of the rangefinders for assessing the suitability of the landing area (see Section IV-B).

A. Obstacle Detection and Avoidance

The LIDAR sensor, which is responsible for the forward view of the MPU-RX4, offers multiple measurements from the platform's surroundings by dividing its total viewing angle into eight equal segments. This comes in contrast to the majority of LIDAR modules which are composed of moving parts to scan the working environment. Therefore, we direct the vehicle toward the least occluded area according to the LIDAR's measurements when an obstacle is recorded. The proposed geofence protection system can address the following two cases.

1) *Static obstacle*: The sensor's measurements correspond to points that remain constant with respect to the world's frame of reference during the flight, e.g., a tall tree.
2) *Dynamic obstacle*: Contrary to the previous category, this case refers to dynamic obstacle that, together with the UAV, also move with respect to the world's frame of reference.

According to the above, the proposed methodology for safe navigation and obstacle avoidance is given below.

1) During its mission, the system retains and constantly reevaluates its position and orientation in real time based on the PX4 autopilot. At the same time, it maintains the predefined trajectory until it reaches the next way-point.
2) As the LIDAR records the environment's surroundings, its data are used to identify any object in its surveillance frustum which might be dangerous to the platform's integrity. Subsequently, a circumference around the obstacle is computed and a safer local path is calculated around the occupied area in the following manner.
   a) *Static obstacle*: An upward-facing 2-D Gaussian curve $N(x, y)$ is computed and placed in the location where the obstacle is detected. By making use of its parameters, the obstacle's opacity circumference can be specified to the desired level of safety, which indicates the local path that the aircraft will follow.
   b) *Dynamic obstacle*: In accordance to previous case, a Gaussian curve is placed over the detected obstacle in a similar manner. Nevertheless, its covariance parameters are calculated based on the obstacle's motion. In this way, we avoid the moving object and define a safe path according to the object's behavior.

For the above two cases, the Gaussian function can be defined as [108]

$$N(x, y) = A \cdot \exp\big(-\big(a(x - x_0)^2 + 2b(x - x_0)(y - y_0) + c(y - y_0)^2\big)\big)$$

where, A denotes the amplitude coefficient, $[x_0, y_0]$ the center of the Gaussian curve, $[\sigma_x, \sigma_y]$ its standard deviation along the two axes X and Y of the world frame of reference and

$$a = \frac{\cos^2\theta}{2\sigma_x^2} + \frac{\sin^2\theta}{2\sigma_y^2} \tag{1}$$

$$b = -\frac{\sin 2\theta}{4\sigma_x^2} + \frac{\sin 2\theta}{4\sigma_y^2} \tag{2}$$

$$c = \frac{\sin^2\theta}{2\sigma_x^2} + \frac{\cos^2\theta}{2\sigma_y^2}. \tag{3}$$

We define θ as the relative angle in which the obstacle is moving with respect to the aircraft, and we compute the vehicle's movement by curving around the Gaussian pdf at a specific A value. By increasing $[\sigma_x, \sigma_y]$ or by decreasing the targeted value of A, the circumference can be broaden according to the desired safety standards. To ensure the proposed platform's integrity, coefficient A is dynamically calculated for each individual obstacle to define a curve 1.5 times wider than the detected object's radius. An illustrative example is presented in Fig. 5.

3) The generated path is transmitted to the navigation system to avoid the possibility of collision. During this process, the previously mentioned steps are constantly

reevaluated so that new potential obstacles can be identified once more.

4) Finally, the platform returns to its predefined trajectory when the obstacle is eventually avoided, while the whole process is reinitialized to continue the environment's monitoring.

B. Autonomous Landing

When the communication between the UAV and the ground station is interrupted, or the system needs to stop its operation due to an unforeseen scenario, autonomous landing is employed through the following steps.

1) The vehicle descends slowly, using the long-range laser rangefinder until it reaches a ground distance of 5 m.
2) The remaining two downward-facing laser rangefinders are activated, and the surface evaluation process begins. To assess the landing area's conditions, i.e., computing the surface's slope and identifying any objects therein, the proposed perception framework uses the sensors' output to calculate the dominant surface's plane.
3) Any object affecting the landing procedure can be detected and avoided by exploiting the aircraft's continuous hovering and consecutive measurements.
4) Based on the above results, the area's slope and clearance are estimated, and the vehicle is prompt to move elsewhere if the terrain is unsuitably steep or anomalous. If the recognized landing surface's conditions are satisfied, the aircraft continues its descending and sensing procedures until it touches the ground.

The approaches for computing the ground's slope and objects therein are described in detail within the following subsections.

1) Landing Surface's Slope Evaluation: Three distance measurements between the UAV and the candidate landing ground are required to calculate a plane. These can be used as distinct points since the sensor's location upon the aircraft's body is known (see Fig. 3). Considering the lengths X and Y from the system's design and that Z_A, Z_B, and Z_Γ are the corresponding sensors' distance measurements, the points needed for the plane's computation are defined for the UAV's frame of reference as

$$P_A = \begin{bmatrix} 0 \\ 0 \\ Z_A \end{bmatrix}, \quad P_B = \begin{bmatrix} X \\ 0 \\ Z_B \end{bmatrix}, \quad P_\Gamma = \begin{bmatrix} X/2 \\ Y \\ Z_\Gamma \end{bmatrix}. \tag{4}$$

By converting the measurements provided from the IMU sensor into a rotation matrix R and assuming no horizontal translation for the vehicle,[7] these points are expressed in the world's frame of reference as

$$P'_A = RP_A, \quad P'_B = RP_B, \quad P'_\Gamma = RP_\Gamma. \tag{5}$$

By employing these data into the general plane equation

$$ax + by + cz + d = 0 \tag{6}$$

each of the parameter a, b, and c is calculated. Note that the last parameter d is set to 0 since it does not affect the plane's slope, just its displacement. The vector $N = [a, b, c]^T$ constitutes the normal vector of the plane, whose angles with respect to the horizontal one are calculated through

$$\cos(\phi) = \frac{N \cdot N_0}{|N||N_0|} \tag{7}$$

where $N_0 = [0, 0, -1]^T$ refers to the normal vector of the horizontal plane. The proposed methodology is summarized in a representative example depicted in Fig. 6.

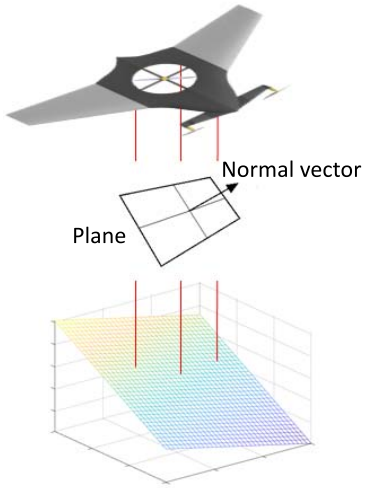

Fig. 6. Process of autonomous landing. When the aircraft reaches an altitude of 5 m, its low-range distance sensors are activated. The data given by these rangefinders and the measurements provided by the long-range sensor are used for computing the ground's dominant plane and, subsequently, its slope.

2) Detection of Protruding Objects: Together with the above detailed procedure for evaluating the ground's slope, the abundance of distance measurements obtained during landing allows us to identify objects protruding from the estimated surface. More specifically, we choose to exploit the hovering movement, which occurs while the aircraft descends to the ground, to gather several measurements from the laser sensors and produce a point cloud of the surface. This cloud is then utilized to identify any object in the candidate landing area using a scheme based on the random sample consensus (RANSAC) algorithm [109]. By keeping a total of 150 consecutive instances, i.e., 150 measurements of points Z_A, Z_B, and Z_Γ, the average distance between the recorded points and each plane is computed. The plane Q with the lowest cost is chosen as the dominant one. Subsequently, outlying points which are located beyond Q are used to identify protruding objects that may harm the platform's integrity during landing.

V. Performance Evaluation Results

In this section, we perform a quantitative evaluation of the performance and effectiveness of our geofence protection system [110]. Moreover, the aerodynamic results from the CFD modeling are presented. Finally, the overall computational complexity, which includes the timing needed for each component to execute, is detailed.

A. Assessing the Platform's Aerodynamics

As the CFD modeling provides the lift and drag forces acting on the UAV for different angles of attack, we obtained

[7] In case of horizontal translations, the respective information can be retrieved by the vehicle's pose estimation module and GNSS measurements.

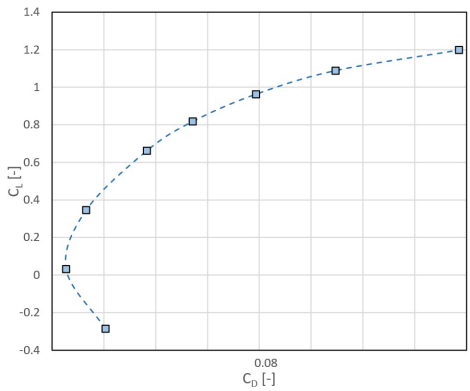

Fig. 7. MPU RX-4 UAV drag polar.

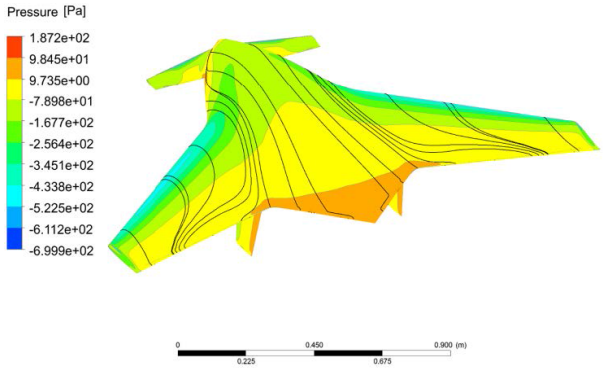

Fig. 8. Pressure distribution around the MPU RX-4 at 12° angle of attack.

TABLE II
AERODYNAMIC PERFORMANCE CHARACTERISTICS OF THE MPU RX-4

	Preliminary design	Final design
Stall speed	25 km/h	25 km/h
Cruise speed	65 km/h	65 km/h
Maximum speed	125 km/h	140 km/h
Endurance	55 minutes	over 60 minutes
$P_{required,cruise}$ / $P_{available}$	15 %	15 %

the drag polar illustrated in Fig. 7. Furthermore, an indicative representation of the pressure distribution and surface streamlines on the UAV at a 12° angle of attack is given in Fig. 8. Based on the above results, an improvement in the aerodynamic characteristics of the UAV is observed compared to the results of the preliminary design. The final aerodynamic performance characteristics of the MPU RX-4 at the end of the detailed design phase are given in Table II.

B. Geofence Protection System Performance

Regarding the proposed geofence protection system, we evaluated whether our approach can select the proper area to navigate when obstacles are presented and if the landing surface's suitability is satisfied. Our experiments were carried out in an outdoor environment using three different surface cases, viz., flat, increased slope, and rocky for evaluating the

TABLE III
SUCCESS RATE OF THE LIDAR. EACH COLUMN REPORTS THE RATE FOR OBJECTS BEING AT A CERTAIN DISTANCE RANGE FROM THE SENSOR. EACH ROW SHOWS THE SUCCESS RATE OF DETECTING OBJECTS SMALLER THAN A CERTAIN SIZE

Size (Centimeters)	Distance (meters)		
	150 m	100 m	50 m
Small (20)	75 %	79 %	82 %
Medium (35)	85 %	88 %	90 %
Large (50)	90 %	92 %	95 %

TABLE IV
ACCURACY OF OUR GEOFENCE PROTECTION SYSTEM TO DETECT OBSTACLES

Distance (meters)	150	100	50	150	100	50
Size (Centimeters)	Mean estimated diameter			Standard deviation		
Small (20)	17 cm	18 cm	19 cm	2.6	2.0	1.0
Medium (35)	30 cm	31 cm	33 cm	2.4	2.4	1.5
Large (50)	46 cm	46 cm	48 cm	2.0	1.9	1.2

latter scenario. Furthermore, we chose to utilize flying balls, as obstacles for assessing the former case to guarantee the integrity of the developed platform.

1) Evaluating the Obstacle Detection Algorithms: For a geofence protection system to be effective, it has to ensure low latency and robustness in terms of success rate; our first analysis regards the system's ability to detect obstacles. Toward this end, we performed a series of experiments using flying balls of different sizes. In particular, we selected sizes of up to 50 cm in diameter, and we grouped them into three different categories: small which represent obstacles of around 20 cm in diameter, medium that correspond to 35 cm, and the large ones for 50 cm. Holding them by a rope, such objects were left swing in the air in front of the sensor's field of view. This way we were able to determine the time window at which they were visible by the system. If the object was in the sensor's field of view but did not report any detection, we considered it a false negative of the detection algorithm. This procedure resulted in the detection success rate reported in Table III. As one can notice, the selected sensor provides a high success rate for each object size. However, the flying balls belonging to the large category showed a higher detection rate at long distances, primarily because of their size, rendering them easier for the system to detect. Additionally, we checked our algorithm's trajectory suggestion, while being disconnected from the vehicle's control module for safety reasons, which yielded the circumference estimation results presented in Table IV.

2) Evaluating the Surface Detection Pipeline: Our platform was tested on two different scenarios [68]. Regarding the first one, we assessed our algorithm on a flat surface without obstacles or a significant slope, i.e., a case for suitable landing. Concerning the second scenario, two different cases were evaluated. The first was a surface that presented an increased slope ($>30°$), whereas the second was a surface with a large

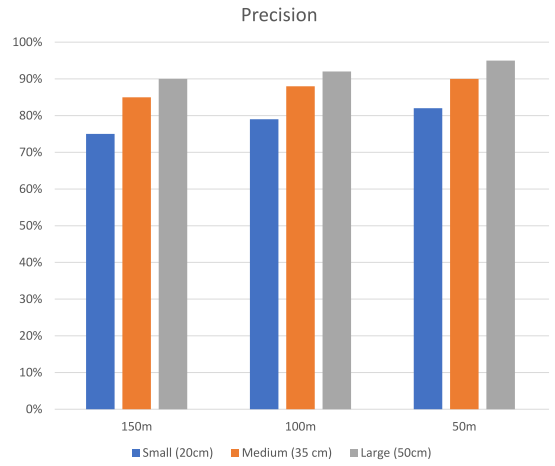

Fig. 9. Detection success rate.

stone which would harm the platform's integrity. During each landing trial, our MPU RX-4 was able to recognize the suitability of the surface conditions. As distance measurements were acquired from the laser rangefinders, they showed a slight deviation due to the grass; however, the system detected the plane's slope with high accuracy due to the proposed RANSAC-based scheme.

Similarly, a set of trials was held to test the detection algorithm when the aircraft encountered an unsuitable ground surface. Regarding the case of an increased slope, a surface at 40° was selected. Our experiments showed that our system could compute the ground's slope with ±5° accuracy during each trial. The landing area presented a large stone therein in the last test case. During each evaluation trial, the system detected that the ground's slope was not flat, canceling its landing process due to the stone's size.

3) Uncertainty Analysis: Aiming to evaluate the uncertainty associated with the measurements provided by the LIDAR sensor, we conducted a similar series of experiments as described above. By capturing a total of 100 distance measurements for each obstacle (e.g., small, medium, and large), in Fig. 9, we illustrate the results presented in Table III. In particular, for each histogram column, we provide the average precision achieved via our measurements. More specifically, during this experiment our intention was to recognize the obstacle. Thus, as a result the segment from which the distance was captured did not affected the evaluation protocol. It is worth noting that the proposed measurement sensor is able to capture the obstacle existence through a high precision score reaching a value over 70% for each case. However, this result is higher as the sensor comes closer to the object, while the environmental conditions are the reason behind a drop in this value.

In a similar manner, aiming to evaluate the sensor's accuracy, we recorded the measurements provided by the LIDAR's different segments to compute the obstacle's size. As shown in Table IV, the generated scores as similar to the detection success rate, i.e., the closest an obstacle the more accurate the measurement. Nevertheless, the standard deviation of the captured values indicate that our sensor detects the obstacle's diameter with high accuracy rendering the aircraft's maneuver more safe.

TABLE V
AVERAGE PROCESSING TIME NEEDED FOR RECOGNIZING THE SURFACE CONDITIONS

		Time (ms)
Sensor data	Long-range range-finder	9.2
	Low-range range-finder (1)	6.5
	Low-range range-finder (2)	6.6
	LIDAR	10.0
Plane computation	Points' rotation	20.2
	Plane computation	40.8
Landing place recognition	Slope computation	10.9
	Robust surface detection	55.8
Obstacle avoidance	Object detection	5.0
	Circumference estimation	1.8
	Flight path computation	0.7
Geofence protection system		165.5

TABLE VI
COMPARATIVE RESULTS

Approach	Kong *et al.* [101]			**Proposed**		
	Obstacle avoidance			Obstacle avoidance		
Obstacle size (cm)	20	35	50	20	35	50
Accuracy (%)	80	88	91	79	88	92
Timing (ms)	26.2	26.2	26.2	7.5	7.5	7.5

4) Overall Complexity: Since real-time constraints must be satisfied for a safe mission, one of the most crucial prerequisites is the system's computational complexity. To quantify the computational cost of our geofence protection system, we evaluated each part of our method individually. Table V shows the results of our evaluation, highlighting the efficiency of each step of the algorithm, described in Section IV. It is worth noting that our system computes the surface conditions at 15.0 Hz and the avoidance flight path at 133.3 Hz. These frequencies satisfy the real-time constraints by detecting hazardous situations faster than the platform's locomotion in each case.

5) Comparative Results: Next, we compare the proposed obstacle avoidance technique with the state-of-the-art approach presented in [101]. Nevertheless, since a source code regarding this pipeline is not publicly available, we implemented the collision check based on the original method in [111]. This version utilizes a set of discrete points along the trajectory by searching its nearest neighbors on a set of time-accumulated k-dimensional trees (KD). If a point on the trajectory is too close (i.e., safety clearance) to the nearest point in the sensor's view, a collision alarm is activated.

In this regard, Table VI contains the obstacles' size, the achieved accuracy, and the average response obtained for each instance. The performance of both systems was measured for a distance of 100 m. This value was selected since it can provide a generic performance value allowing both systems to achieve high accuracy in every evaluation obstacle size. During this experiment, our intention was to measure the accuracy as well as the timing needed for each algorithm to detect and compute an obstacle avoidance path. As can be observed, the difference in terms of accuracy is minimum and,

in general, the two methods perform quite similarly. However, our approach is able to process each measurement in lessen time using a reduced set of calculation as compared to the KD-tree approach in [101]. Moreover, we have to note that a comparison with camera-based architectures for obstacle detection and avoidance is not presented since, during our tests, the used companion computer was not able to process images in real time, even by considering only key frames.

VI. Conclusion

As the development of effective perception algorithms to protect the integrity of a UAV's platform is a critical challenge in robotics research and a highly valued goal in industry, in this article, we designed a low-complexity geofence protection system based on low latency sensors. UAVs are equipped with flight-critical sensors to monitor the surrounding environment. The proposed framework pipeline can be adapted to small and light aircraft using the distance measurements provided by three laser rangefinders mounted on the platform's underbelly and the measurements given by a forward-facing LIDAR. We demonstrate the effectiveness of our approach, using only onboard sensing and computation, in an extensive evaluation protocol over a testbed VTOL UAV aircraft. The entire avoidance framework can run in real time on a small computing module onboard the vehicle, together with the entire software stack necessary to let the platform fly. Our approach prioritizes computation, while still providing adequate accuracy, achieving 166 ms at most for computing each necessary step of the procedure.

Acknowledgment

The authors would like to thank the IEEE Transactions on Instrumentation and Measurement editorial team, including the editor-in-chief Ruqiang Yan, an associate editor, and all the reviewers, for their prompt, valuable, and constructive feedback, which largely improved the quality of this article.

References

[1] N. Pessanha Santos, V. Lobo, and A. Bernardino, "Two-stage 3D model-based UAV pose estimation: A comparison of methods for optimization," *J. Field Robot.*, vol. 37, no. 4, pp. 580–605, Jun. 2020.

[2] B. Canis, *Unmanned Aircraft Systems (UAS): Commercial Outlook for a New Industry*. Washington, DC, USA: Congressional Research Service, 2015.

[3] K. P. Valavanis, *Advances in Unmanned Aerial Vehicles: State of the Art and the Road to Autonomy*. Dordrecht, The Netherlands: Springer, 2008.

[4] K. P. Valavanis and G. J. Vachtsevanos, *Handbook of Unmanned Aerial Vehicles*, vol. 1. Dordrecht, The Netherlands: Springer, 2015.

[5] M. A. Khan, W. Ectors, T. Bellemans, D. Janssens, and G. Wets, "UAV-based traffic analysis: A universal guiding framework based on literature survey," *Transp. Res. Proc.*, vol. 22, pp. 541–550, Jan. 2017.

[6] D. Reiser, D. S. Paraforos, M. T. Khan, H. W. Griepentrog, and M. Vázquez-Arellano, "Autonomous field navigation, data acquisition and node location in wireless sensor networks," *Precis. Agricult.*, vol. 18, no. 3, pp. 279–292, Jun. 2017.

[7] S. S. C. Congress, A. J. Puppala, and C. L. Lundberg, "Total system error analysis of UAV-CRP technology for monitoring transportation infrastructure assets," *Eng. Geol.*, vol. 247, pp. 104–116, Dec. 2018.

[8] T. Giitsidis, E. G. Karakasis, A. Gasteratos, and G. C. Sirakoulis, "Human and fire detection from high altitude UAV images," in *Proc. 23rd Euromicro Int. Conf. Parallel, Distrib., Netw.-Based Process.*, Mar. 2015, pp. 309–315.

[9] M. M. Marques et al., "An unmanned aircraft system for maritime operations: The automatic detection subsystem," *Mar. Technol. Soc. J.*, vol. 55, no. 1, pp. 38–49, 2021.

[10] M. Rossi and D. Brunelli, "Autonomous gas detection and mapping with unmanned aerial vehicles," *IEEE Trans. Instrum. Meas.*, vol. 65, no. 4, pp. 765–775, Apr. 2016.

[11] R. S. de Moraes and E. P. de Freitas, "Multi-UAV based crowd monitoring system," *IEEE Trans. Aerosp. Electron. Syst.*, vol. 56, no. 2, pp. 1332–1345, Apr. 2020.

[12] B. D. Song, K. Park, and J. Kim, "Persistent UAV delivery logistics: MILP formulation and efficient heuristic," *Comput. Ind. Eng.*, vol. 120, pp. 418–428, Jun. 2018.

[13] I. T. Papapetros, V. Balaska, and A. Gasteratos, "Multi-layer map: Augmenting semantic visual memory," in *Proc. Int. Conf. Unmanned Aircr. Syst. (ICUAS)*, Sep. 2020, pp. 1206–1212.

[14] R. Fan, J. Jiao, J. Pan, H. Huang, S. Shen, and M. Liu, "Real-time dense stereo embedded in a UAV for road inspection," in *Proc. IEEE/CVF Conf. Comput. Vis. Pattern Recognit. Workshops (CVPRW)*, Long Beach, CA, USA, Jun. 2019, pp. 1–9.

[15] M. Banić, A. Miltenović, M. Pavlović, and I. Ćirić, "Intelligent machine vision based railway infrastructure inspection and monitoring using UAV," *Facta Univ., Ser., Mech. Eng.*, vol. 17, no. 3, pp. 357–364, 2019.

[16] R. Andersen, L. Nalpantidis, O. Ravn, and E. Boukas, "Investigating deep learning architectures towards autonomous inspection for marine classification," in *Proc. IEEE Int. Symp. Saf., Secur., Rescue Robot. (SSRR)*, Nov. 2020, pp. 197–204.

[17] L. Yang, J. Fan, Y. Liu, E. Li, J. Peng, and Z. Liang, "A review on state-of-the-art power line inspection techniques," *IEEE Trans. Instrum. Meas.*, vol. 69, no. 12, pp. 9350–9365, Dec. 2020.

[18] H. Zhang et al., "Attention-guided multitask convolutional neural network for power line parts detection," *IEEE Trans. Instrum. Meas.*, vol. 71, pp. 1–13, 2022.

[19] E. Lygouras, N. Santavas, A. Taitzoglou, K. Tarchanidis, A. Mitropoulos, and A. Gasteratos, "Unsupervised human detection with an embedded vision system on a fully autonomous UAV for search and rescue operations," *Sensors*, vol. 19, no. 16, p. 3542, Aug. 2019.

[20] V. A. Feraru, R. E. Andersen, and E. Boukas, "Towards an autonomous UAV-based system to assist search and rescue operations in man overboard incidents," in *Proc. IEEE Int. Symp. Saf., Secur., Rescue Robot. (SSRR)*, Nov. 2020, pp. 57–64.

[21] K. E. Wenzel, A. Masselli, and A. Zell, "Automatic take off, tracking and landing of a miniature UAV on a moving carrier vehicle," *J. Intell. Robot. Syst.*, vol. 61, nos. 1–4, pp. 221–238, Jan. 2011.

[22] N. P. Santos, V. Lobo, and A. Bernardino, "Directional statistics for 3D model-based UAV tracking," *IEEE Access*, vol. 8, pp. 33884–33897, 2020.

[23] K. A. Tsintotas, L. Bampis, and A. Gasteratos, "The revisiting problem in simultaneous localization and mapping," in *Online Appearance-Based Place Recognition and Mapping*. Cham, Switzerland: Springer, 2022, pp. 1–33.

[24] N. P. Santos, V. Lobo, and A. Bernardino, "Autoland project: Fixed-wing UAV landing on a fast patrol boat using computer vision," in *Proc. IEEE OCEANS*, Oct. 2019, pp. 1–5.

[25] J. Farrell and M. Barth, *The Global Positioning System and Inertial Navigation*, vol. 61. New York, NY, USA: McGraw-Hill, 1999.

[26] T. Baca, P. Stepan, and M. Saska, "Autonomous landing on a moving car with unmanned aerial vehicle," in *Proc. Eur. Conf. Mobile Robots (ECMR)*, Sep. 2017, pp. 1–6.

[27] C.-S. Yoo and I.-K. Ahn, "Low cost GPS/INS sensor fusion system for UAV navigation," in *Proc. Digit. Avionics Syst. Conf.*, vol. 2, 2003, p. 8.

[28] O. Kardoudi, "Hawk attacks drone in a battle of claw versus machine," Gizmodo. [Online]. Available: https://gizmodo.com/hawk-attacks-a-drone-mid-air-bringing-it-down-to-the-gr-1644785744

[29] M. Reporter, "When eagles attack! drone camera mistaken for rival," Daily Mail, London, U.K., Jan. 2016. [Online]. Available: https://www.dailymail.co.uk/video/news/video-1154408/Golden-Eagle-attacks-drone-camera-mistaking-rival.html

[30] D. Falanga, K. Kleber, and D. Scaramuzza, "Dynamic obstacle avoidance for quadrotors with event cameras," *Sci. Robot.*, vol. 5, no. 40, Mar. 2020, Art. no. eaaz9712.

[31] M. Veismann, C. Dougherty, and M. Gharib, "Experimental studies of the rotor flow downwash on the stability of multi-rotor crafts in descent," in *Proc. APS Division Fluid Dyn. Meeting Abstr.*, 2017, p. M18.002. [Online]. Available: https://ui.adsabs.harvard.edu/abs/2017APS..DFDM18002V/exportcitation

[32] B. Herissé, T. Hamel, R. Mahony, and F.-X. Russotto, "Landing a VTOL unmanned aerial vehicle on a moving platform using optical flow," *IEEE Trans. Robot.*, vol. 28, no. 1, pp. 77–89, Feb. 2012.

[33] T. Mitroudas, K. A. Tsintotas, N. Santavas, A. Psomoulis, and A. Gasteratos, "Towards 3D printed modular unmanned aerial vehicle development: The landing safety paradigm," in *Proc. IEEE Int. Conf. Imag. Syst. Techn. (IST)*, Jun. 2022, pp. 1–6.

[34] M. Hamanaka and F. Nakano, "Surface-condition detection system of drone-landing space using ultrasonic waves and deep learning," in *Proc. Int. Conf. Unmanned Aircr. Syst. (ICUAS)*, Sep. 2020, pp. 1452–1459.

[35] S. Lee, T. Shim, S. Kim, J. Park, K. Hong, and H. Bang, "Vision-based autonomous landing of a multi-copter unmanned aerial vehicle using reinforcement learning," in *Proc. Int. Conf. Unmanned Aircr. Syst. (ICUAS)*, Jun. 2018, pp. 108–114.

[36] Z. Wu et al., "Autonomous UAV landing system based on visual navigation," in *Proc. IEEE Int. Conf. Imag. Syst. Techn. (IST)*, Dec. 2019, pp. 1–6.

[37] E. Narváez, A. A. Ravankar, A. Ravankar, T. Emaru, and Y. Kobayashi, "Autonomous VTOL-UAV docking system for heterogeneous multirobot team," *IEEE Trans. Instrum. Meas.*, vol. 70, pp. 1–18, 2021.

[38] B. Abou Merhy, P. Payeur, and E. M. Petriu, "Application of segmented 2-D probabilistic occupancy maps for robot sensing and navigation," *IEEE Trans. Instrum. Meas.*, vol. 57, no. 12, pp. 2827–2837, Dec. 2008.

[39] K. A. Tsintotas, L. Bampis, and A. Gasteratos, "The revisiting problem in simultaneous localization and mapping: A survey on visual loop closure detection," *IEEE Trans. Intell. Transp. Syst.*, vol. 23, no. 11, pp. 19929–19953, Nov. 2022.

[40] M. B. Vankadari, K. Das, C. Shinde, and S. Kumar, "A reinforcement learning approach for autonomous control and landing of a quadrotor," in *Proc. Int. Conf. Unmanned Aircr. Syst. (ICUAS)*, Jun. 2018, pp. 676–683.

[41] K. A. Tsintotas, L. Bampis, and A. Gasteratos, "Assigning visual words to places for loop closure detection," in *Proc. IEEE Int. Conf. Robot. Autom. (ICRA)*, May 2018, pp. 5979–5985.

[42] J. S. Wynn and T. W. McLain, "Visual servoing for multirotor precision landing in daylight and after-dark conditions," in *Proc. Int. Conf. Unmanned Aircr. Syst. (ICUAS)*, Jun. 2019, pp. 1242–1248.

[43] S. Sun, Y. Yin, X. Wang, and D. Xu, "Robust visual detection and tracking strategies for autonomous aerial refueling of UAVs," *IEEE Trans. Instrum. Meas.*, vol. 68, no. 12, pp. 4640–4652, Dec. 2019.

[44] Y. Wang, H. Wang, B. Liu, Y. Liu, J. Wu, and Z. Lu, "A visual navigation framework for the aerial recovery of UAVs," *IEEE Trans. Instrum. Meas.*, vol. 70, pp. 1–13, 2021.

[45] Y. Bi and H. Duan, "Implementation of autonomous visual tracking and landing for a low-cost quadrotor," *Optik, Int. J. Light Electron Opt.*, vol. 124, no. 18, pp. 3296–3300, Sep. 2013.

[46] K. A. Tsintotas, L. Bampis, S. Rallis, and A. Gasteratos, "SeqSLAM with bag of visual words for appearance based loop closure detection," in *Proc. Int. Conf. Robot. Alpe-Adria Danube Reg.*, 2018, pp. 580–587.

[47] K. A. Tsintotas, L. Bampis, and A. Gasteratos, "Probabilistic appearance-based place recognition through bag of tracked words," *IEEE Robot. Autom. Lett.*, vol. 4, no. 2, pp. 1737–1744, Apr. 2019.

[48] R. Fan, J. Jiao, H. Ye, Y. Yu, I. Pitas, and M. Liu, "Key ingredients of self-driving cars," in *Proc. EUSIPCO Satell. Workshop, Signal Process., Comput. Vis. Deep Learn. Auton. Syst.*, A Coruña, Spain, Sep. 2019.

[49] K. A. Tsintotas, L. Bampis, and A. Gasteratos, "Tracking-DOSeqSLAM: A dynamic sequence-based visual place recognition paradigm," *IET Comput. Vis.*, vol. 15, no. 4, pp. 258–273, Jun. 2021.

[50] K. A. Tsintotas, L. Bampis, and A. Gasteratos, "Modest-vocabulary loop-closure detection with incremental bag of tracked words," *Robot. Auto. Syst.*, vol. 141, Jul. 2021, Art. no. 103782.

[51] K. A. Tsintotas, L. Bampis, and A. Gasteratos, "DOSeqSLAM: Dynamic on-line sequence based loop closure detection algorithm for SLAM," in *Proc. IEEE Int. Conf. Imag. Syst. Techn. (IST)*, Oct. 2018, pp. 1–6.

[52] K. A. Tsintotas, P. Giannis, L. Bampis, and A. Gasteratos, "Appearance-based loop closure detection with scale-restrictive visual features," in *Proc. Int. Conf. Comput. Vis. Syst.*, 2019, pp. 75–87.

[53] L. Zhu, S. Zhang, X. Wang, S. Chen, H. Zhao, and D. Wei, "Multilevel recognition of UAV-to-ground targets based on micro-Doppler signatures and transfer learning of deep convolutional neural networks," *IEEE Trans. Instrum. Meas.*, vol. 70, pp. 1–11, 2020.

[54] S. Saripalli, J. F. Montgomery, and G. S. Sukhatme, "Visually guided landing of an unmanned aerial vehicle," *IEEE Trans. Robot. Autom.*, vol. 19, no. 3, pp. 371–380, Jun. 2003.

[55] X. Yang, H. Pota, M. Garratt, and V. Ugrinovskii, "Prediction of vertical motions for landing operations of UAVs," in *Proc. 47th IEEE Conf. Decis. Control*, Dec. 2008, pp. 5048–5053.

[56] L. Jiang, Z. Guo, and B. Zhang, "Scalar calibration of aeromagnetic data using BPANN and LS algorithms based on fixed-wing UAV platform," *IEEE Trans. Instrum. Meas.*, vol. 64, no. 7, pp. 1968–1976, Jul. 2015.

[57] W. Kong, D. Zhou, D. Zhang, and J. Zhang, "Vision-based autonomous landing system for unmanned aerial vehicle: A survey," in *Proc. Int. Conf. Multisensor Fusion Inf. Integr. Intell. Syst. (MFI)*, Sep. 2014, pp. 1–8.

[58] S. An, H. Zhu, D. Wei, K. A. Tsintotas, and A. Gasteratos, "Fast and incremental loop closure detection with deep features and proximity graphs," *J. Field Robot.*, vol. 39, no. 4, pp. 473–493, Jun. 2022.

[59] M. F. B. Ramli, S. S. Shamsudin, and A. Legowo, "Safe avoidance path detection using multi sensor integration for small unmanned aerial vehicle," in *Proc. 5th IEEE Int. Workshop Metrol. Aerosp. (MetroAeroSpace)*, Jun. 2018, pp. 101–106.

[60] D. Burton, D. B. Dunlap, L. J. Wood, and P. P. Flaig, "LiDAR intensity as a remote sensor of rock properties," *J. Sedimentary Res.*, vol. 81, no. 5, pp. 339–347, May 2011.

[61] A. F. C. Errington, B. L. F. Daku, and A. F. Prugger, "Reflectance modelling using terrestrial LiDAR intensity data," in *Proc. IEEE Int. Conf. Imag. Syst. Techn. (IST)*, Sep. 2015, pp. 1–6.

[62] D. Ghorpade, A. D. Thakare, and S. Doiphode, "Obstacle detection and avoidance algorithm for autonomous mobile robot using 2D LiDAR," in *Proc. Int. Conf. Comput., Commun., Control Autom. (ICCUBEA)*, Aug. 2017, pp. 1–6.

[63] A. Moffatt, E. Platt, B. Mondragon, A. Kwok, D. Uryeu, and S. Bhandari, "Obstacle detection and avoidance system for small UAVs using a LiDAR," in *Proc. Int. Conf. Unmanned Aircr. Syst. (ICUAS)*, Sep. 2020, pp. 633–640.

[64] Y. F. He, Y. Peng, S. J. Wang, D. T. Liu, and P. H. W. Leong, "A structured sparse subspace learning algorithm for anomaly detection in UAV flight data," *IEEE Trans. Instrum. Meas.*, vol. 67, no. 1, pp. 90–100, Jan. 2018.

[65] Y. He, Y. Peng, S. Wang, and D. Liu, "ADMOST: UAV flight data anomaly detection and mitigation via online subspace tracking," *IEEE Trans. Instrum. Meas.*, vol. 68, no. 4, pp. 1035–1044, Apr. 2019.

[66] W. Youn, H. Choi, A. Cho, S. Kim, and M. B. Rhudy, "Accelerometer fault-tolerant model-aided state estimation for high-altitude long-endurance UAV," *IEEE Trans. Instrum. Meas.*, vol. 69, no. 10, pp. 8539–8553, Oct. 2020.

[67] B. K. Wang, X. Y. Peng, M. Jiang, and D. T. Liu, "Real-time fault detection for UAV based on model acceleration engine," *IEEE Trans. Instrum. Meas.*, vol. 69, no. 12, pp. 9505–9516, Dec. 2020.

[68] K. A. Tsintotas, L. Bampis, A. Taitzoglou, I. Kansizoglou, and A. Gasteratos, "Safe UAV landing: A low-complexity pipeline for surface conditions recognition," in *Proc. IEEE Int. Conf. Imag. Syst. Techn. (IST)*, Aug. 2021, pp. 1–6.

[69] K. A. Tsintotas, L. Bampis, and A. Gasteratos, "Open challenges and conclusion," in *Online Appearance-Based Place Recognition and Mapping*. Cham, Switzerland: Springer, 2022, pp. 97–111.

[70] P. E. Kaparos, C. D. Bliamis, and K. Yakinthos, "Conceptual design of a UAV with VTOL characteristics," in *Proc. AIAA Aviation Forum*, Jun. 2019, p. 3137.

[71] C. Bliamis, I. Zacharakis, P. Kaparos, and K. Yakinthos, "Aerodynamic and stability analysis of a VTOL flying wing UAV," *IOP Conf. Ser., Mater. Sci. Eng.*, vol. 1024, no. 1, Jan. 2021, Art. no. 012039.

[72] K. Muraoka, N. Okada, and D. Kubo, "Quad tilt wing VTOL UAV: Aerodynamic characteristics and prototype flight," in *Proc. AIAA Infotech@Aerospace Conf.*, Apr. 2009, p. 1834.

[73] Ö. Dündar, M. Bilici, and T. Ünler, "Design and performance analyses of a fixed wing battery VTOL UAV," *Eng. Sci. Technol., Int. J.*, vol. 23, no. 5, pp. 1182–1193, Oct. 2020.

[74] A. S. Saeed, A. B. Younes, C. Cai, and G. Cai, "A survey of hybrid unmanned aerial vehicles," *Progr. Aerosp. Sci.*, vol. 98, pp. 91–105, Apr. 2018.

[75] M. Tielin, Y. Chuanguang, G. Wenbiao, X. Zihan, Z. Qinling, and Z. Xiaoou, "Analysis of technical characteristics of fixed-wing VTOL UAV," in *Proc. IEEE Int. Conf. Unmanned Syst. (ICUS)*, Oct. 2017, pp. 293–297.

[76] M. Tyan, N. V. Nguyen, S. Kim, and J.-W. Lee, "Comprehensive preliminary sizing/resizing method for a fixed wing—VTOL electric UAV," *Aerosp. Sci. Technol.*, vol. 71, pp. 30–41, Dec. 2017.

[77] C. Chen, J. Y. Zhang, D. B. Zhang, and L. C. Shen, "Control and flight test of a tilt-rotor unmanned aerial vehicle," *Int. J. Adv. Robot. Syst.*, vol. 14, no. 1, pp. 1–12, Jan. 2017.

[78] M. Simon, L. CopăCean, C. Popescu, and L. Cojocariu, "3D mapping of a village with a WingtraOne VTOL tailsiter drone using Pix4D mapper," *Res. J. Agr. Sci.*, vol. 53, no. 2, pp. 1–10, 2021.
[79] D. Mitridis, C. Bliamis, P. Kaparos, and K. Yakinthos, "Design of a tilting mechanism for a VTOL flying wing UAV," *IOP Conf. Ser., Mater. Sci. Eng.*, vol. 1024, no. 1, 2021, Art. no. 012056.
[80] S. An, F. Zhou, M. Yang, H. Zhu, C. Fu, and K. A. Tsintotas, "Real-time monocular human depth estimation and segmentation on embedded systems," in *Proc. IEEE/RSJ Int. Conf. Intell. Robots Syst. (IROS)*, Sep. 2021, pp. 55–62.
[81] D. Falanga, S. Kim, and D. Scaramuzza, "How fast is too fast? The role of perception latency in high-speed sense and avoid," *IEEE Robot. Autom. Lett.*, vol. 4, no. 2, pp. 1884–1891, Apr. 2019.
[82] K. A. Tsintotas, V. Sevetlidis, I. T. Papapetros, V. Balaska, A. Psomoulis, and A. Gasteratos, "BK tree indexing for active vision-based loop-closure detection in autonomous navigation," in *Proc. 30th Medit. Conf. Control Autom. (MED)*, Jun. 2022, pp. 532–537.
[83] K. A. Tsintotas, S. An, I. T. Papapetros, F. K. Konstantinidis, G. C. Sirakoulis, and A. Gasteratos, "Dimensionality reduction through visual data resampling for low-storage loop-closure detection," in *Proc. IEEE Int. Conf. Imag. Syst. Techn. (IST)*, Jun. 2022, pp. 1–6.
[84] O. Esrafilian and H. D. Taghirad, "Autonomous flight and obstacle avoidance of a quadrotor by monocular SLAM," in *Proc. 4th Int. Conf. Robot. Mechatronics (ICROM)*, Oct. 2016, pp. 240–245.
[85] H. Alvarez, L. M. Paz, J. Sturm, and D. Cremers, "Collision avoidance for quadrotors with a monocular camera," in *Experimental Robotics*, M. A. Hsieh, O. Khatib, and V. Kumar, Eds. Cham, Switzerland: Springer, 2016, pp. 195–209.
[86] Y. Lin et al., "Autonomous aerial navigation using monocular visual-inertial fusion," *J. Field Robot.*, vol. 35, no. 1, pp. 23–51, Jan. 2018.
[87] K. A. Tsintotas, L. Bampis, S. An, G. F. Fragulis, S. G. Mouroutsos, and A. Gasteratos, "Sequence-based mapping for probabilistic visual loop-closure detection," in *Proc. IEEE Int. Conf. Imag. Syst. Techn. (IST)*, Aug. 2021, pp. 1–6.
[88] H. Oleynikova, D. Honegger, and M. Pollefeys, "Reactive avoidance using embedded stereo vision for MAV flight," in *Proc. IEEE Int. Conf. Robot. Autom. (ICRA)*, May 2015, pp. 50–56.
[89] M. Burri, H. Oleynikova, M. W. Achtelik, and R. Siegwart, "Real-time visual-inertial mapping, re-localization and planning onboard MAVs in unknown environments," in *Proc. IEEE/RSJ Int. Conf. Intell. Robots Syst. (IROS)*, Sep. 2015, pp. 1872–1878.
[90] K. Mohta et al., "Fast, autonomous flight in GPS-denied and cluttered environments," *J. Field Robot.*, vol. 35, no. 1, pp. 101–120, 2018.
[91] A. J. Barry, P. R. Florence, and R. Tedrake, "High-speed autonomous obstacle avoidance with pushbroom stereo," *J. Field Robot.*, vol. 35, no. 1, pp. 52–68, Jan. 2018.
[92] S. Liu, M. Watterson, S. Tang, and V. Kumar, "High speed navigation for quadrotors with limited onboard sensing," in *Proc. IEEE Int. Conf. Robot. Autom. (ICRA)*, May 2016, pp. 1484–1491.
[93] B. T. Lopez and J. P. How, "Aggressive 3-D collision avoidance for high-speed navigation," in *Proc. IEEE Int. Conf. Robot. Autom. (ICRA)*, May 2017, pp. 5759–5765.
[94] A. S. Huang et al., "Visual odometry and mapping for autonomous flight using an RGB-D camera," in *Robotics Research*, H. I. Christensen and O. Khatib, Eds. Cham, Switzerland: Springer, 2017, pp. 235–252.
[95] E. Ackerman, "Skydio demonstrates incredible obstacle-dodging full autonomy with new R1 consumer drone," *IEEE Spectr.*, Feb. 2018.
[96] G. Gallego et al., "Event-based vision: A survey," *IEEE Trans. Pattern Anal. Mach. Intell.*, vol. 44, no. 1, pp. 154–180, Jan. 2022.
[97] L. Salt and D. Howard, "Self-adaptive differential evolution for bio-inspired neuromorphic collision avoidance," *CoRR*, vol. abs/1704.04853, pp. 1–8, Apr. 2017.
[98] A. Mitrokhin, C. Fermüller, C. Parameshwara, and Y. Aloimonos, "Event-based moving object detection and tracking," in *Proc. IEEE/RSJ Int. Conf. Intell. Robots Syst. (IROS)*, Oct. 2018, pp. 1–9.
[99] M. B. Milde, O. J. N. Bertrand, H. Ramachandran, M. Egelhaaf, and E. Chicca, "Spiking elementary motion detector in neuromorphic systems," *Neural Comput.*, vol. 30, no. 9, pp. 2384–2417, Sep. 2018.
[100] J. Villa, J. Aaltonen, and K. T. Koskinen, "Path-following with LiDAR-based obstacle avoidance of an unmanned surface vehicle in harbor conditions," *IEEE/ASME Trans. Mechatronics*, vol. 25, no. 4, pp. 1812–1820, Aug. 2020.
[101] F. Kong, W. Xu, Y. Cai, and F. Zhang, "Avoiding dynamic small obstacles with onboard sensing and computation on aerial robots," *IEEE Robot. Autom. Lett.*, vol. 6, no. 4, pp. 7869–7876, Oct. 2021.
[102] F. Fuschini et al., "An UAV-based experimental setup for propagation characterization in urban environment," *IEEE Trans. Instrum. Meas.*, vol. 70, pp. 1–11, 2021.
[103] J. Roskam, *Airplane Design VII: Determination of Stability, Control and Performance Characteristics: FAR and Military Requirements*, vol. 1. Lawrence, KS, USA: DARcorporation, 1985.
[104] P. Spalart and S. Allmaras, "A one-equation turbulence model for aerodynamic flows," in *Proc. 30th Aerosp. Sci. Meeting Exhibit*, Jan. 1992, p. 439.
[105] P. Kaparos, C. Papadopoulos, and K. Yakinthos, "Conceptual design methodology of a box wing aircraft: A novel commercial airliner," *Proc. Inst. Mech. Eng. G, J. Aerosp. Eng.*, vol. 232, no. 14, pp. 2651–2662, Nov. 2018.
[106] V. Somashekar and A. I. S. Raj, "Comparative study on the prediction of aerodynamic characteristics of mini–unmanned aerial vehicle with turbulence models," *Int. J. Aviation, Aeronaut., Aerosp.*, vol. 8, no. 1, p. 7, 2021.
[107] C. L. Rumsey and P. R. Spalart, "Turbulence model behavior in low Reynolds number regions of aerodynamic flowfields," *AIAA J.*, vol. 47, no. 4, pp. 982–993, Apr. 2009.
[108] N. Nawri, "Berechnung von kovarianzellipsen," Karlsruher Institut Technologief, Karlsruhe, Germany, Tech. Rep., 1996.
[109] F. Mufti, R. Mahony, and J. Heinzmann, "Robust estimation of planar surfaces using spatio-temporal RANSAC for applications in autonomous vehicle navigation," *Robot. Auto. Syst.*, vol. 60, no. 1, pp. 16–28, Jan. 2012.
[110] K. A. Tsintotas, L. Bampis, and A. Gasteratos, "Benchmarking," in *Online Appearance-Based Place Recognition and Mapping*. Cham, Switzerland: Springer, 2022, pp. 35–43.
[111] B. Zhou, F. Gao, L. Wang, C. Liu, and S. Shen, "Robust and efficient quadrotor trajectory generation for fast autonomous flight," *IEEE Robot. Autom. Lett.*, vol. 4, no. 4, pp. 3529–3536, Oct. 2019.

Konstantinos A. Tsintotas (Senior Member, IEEE) received the bachelor's degree from the Department of Automation, Technological Education Institute of Chalkida, Psachna, Greece, in 2010, the master's degree in mechatronics from the Department of Electrical Engineering, Technological Education Institute of Western Macedonia, Kila Kozanis, Greece, in 2015, and the Ph.D. degree in robotics from the Department of Production and Management Engineering, Democritus University of Thrace, Xanthi, Greece, in 2021.

He is currently a Post-Doctoral Researcher with the Laboratory of Robotics and Automation, Department of Production and Management Engineering, Democritus University of Thrace. His work is supported by several research projects funded by the European Commission and the Greek Government. His research interests include vision-based methods for modern and intelligent mechatronics systems. More details are available at: https://robotics.pme.duth.gr/ktsintotas.

Loukas Bampis received the Diploma degree in electrical and computer engineering and the Ph.D. degree in machine vision and embedded systems from the Democritus University of Thrace, Xanthi, Greece, in 2013 and 2019, respectively.

His work has been supported through several research projects funded by the European Space Agency, the European Commission, and the Greek Government. He is currently an Assistant Professor with the Laboratory of Mechatronics and Systems Automation, Department of Electrical and Computer Engineering, Democritus University of Thrace. His research interests include cognitive mechatronics and real-time localization for robotic systems. More details are available at https://utopia.duth.gr/lbampis/.

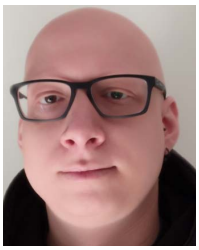

Anastasios Taitzoglou received the Diploma degree from the Department of Production and Management Engineering, Democritus University of Thrace, Xanthi, Greece, in 2019, where he is currently pursuing the Ph.D. degree with the Laboratory of Robotics and Automation, supervised by Professor Antonios Gasteratos.

His research interests include natural language processing, computer vision, and deep reinforcement learning.

Ioannis Kansizoglou received the Diploma degree in electrical and computer engineering from the Aristotle University of Thessaloniki, Thessaloniki, Greece, in 2017, and the Ph.D. degree in deep representation learning and computer vision from the Laboratory of Robotics and Automation, Department of Production and Management Engineering, Democritus University of Thrace, Xanthi, Greece, in 2021.

He is currently a Post-Doctoral Researcher with the Laboratory of Robotics and Automation, Department of Production and Management Engineering, Democritus University of Thrace. His research interests include deep representation learning, emotion analysis, and human–robot interaction. His work is supported by several research projects funded by the European Commission and the Greek Government. More details are available at: https://robotics.pme.duth.gr/ikansi.

Pavlos Kaparos received the Diploma degree from the Mechanical Engineering Department, Aristotle University of Thessaloniki (AUTh), Thessaloniki, Greece, in 2014, where he is currently pursuing the Ph.D. degree with the Fluid Mechanics and Turbomachinery Laboratory.

He is also a Researcher at the AUTh UAV-Integrated Research Center. His research interests include UAV and aircraft design and performance, innovative VTOL fixed-wing UAV concepts, advanced CFD modeling, experimental fluid mechanics, and plasma active flow control techniques. Furthermore, he has applied experience in UAV design, development, integration, and flight testing, having been heavily involved in the projects of HCUAV, DELAER, and MPU funded by the Greek Government. At the same time, he also has year-long experience in novel aero engines and aircraft design projects, such as FP7 LEMCOTEC and H2020 ULTIMATE.

Chris Bliamis received the Diploma degree from the Mechanical Engineering Department, Aristotle University of Thessaloniki, Thessaloniki, Greece, in 2019, where he is currently pursuing the Ph.D. degree with the Fluid Mechanics and Turbomachinery Laboratory.

He is also a Researcher at the AUTh UAV-Integrated Research Center. His research interests include advanced CFD modeling techniques, passive flow control techniques, experimental fluid mechanics, supersonic aircraft design and performance, and innovative VTOL fixed-wing UAV concepts. He also has year-long applied experience in projects related to UAV design, integration, and flight testing, as well as passive flow control techniques, having been involved in the DELAER, MPU, and RADAERO research projects.

Kyros Yakinthos is currently a Professor with the Fluid Mechanics and Turbomachinery Laboratory, Department of Mechanical Engineering, Aristotle University of Thessaloniki (AUTh), Thessaloniki, Greece. His scientific expertise is mainly focused on the aircraft and UAV conceptual design and performance assessment, fluid mechanics, advanced CFD modeling, and innovative aero-engine architectures and concepts. He has authored more than 120 scientific papers in journals and international conferences related to aeronautics and propulsion. In addition, he has been involved in various European research projects, cofunded by the European Industry and the European Commission, such as the FP5 AEROHEX, FP6 NEWAC, FP7 LEMCOTEC, and H2020 ULTIMATE projects. Furthermore, he was the Coordinator and the Chief Engineer of the HCUAV project, cofunded by Greek companies and National and European funds, involving designing and manufacturing a fixed-wing MALE UAV prototype developed for civil operations in Greece. He is also the co-inventor of a joint patent with MTU Aero Engines A.G. for innovative compact heat exchangers. He is the Coordinator and the Chief Engineer of projects funded by the Greek Government and the Greek industry for designing, manufacturing, and testing fixed-wing UAVs covering small- and large-scale/range/endurance missions over sea and land.

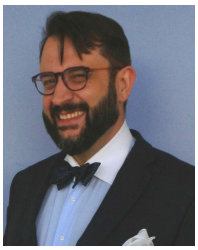

Antonios Gasteratos (Senior Member, IEEE) received the M.Eng. and Ph.D. degrees from the Department of Electrical and Computer Engineering, Democritus University of Thrace (DUTh), Xanthi, Greece, in 1994 and 1998, respectively.

From 1999 to 2000, he was a Visiting Researcher with the Laboratory of Integrated Advanced Robotics (LIRALab), DIST, University of Genoa, Genoa, Italy. He is currently a Professor and the Head of the Production and Management Engineering Department, DUTh. He is also the Director of the Laboratory of Robotics and Automation, DUTh, and teaches courses in robotics, automatic control systems, electronics, mechatronics, and computer vision. He has authored more than 220 papers in books, journals, and conferences. His research interests include mechatronics and robot vision.

Dr. Gasteratos is a Fellow member of IET. He has served as a reviewer for numerous scientific journals and international conferences. He is a Subject Editor of *Electronics Letters* and an Associate Editor of the *International Journal of Optomecatronics*. He has organized/co-organized several international conferences. More details about him are available at http://robotics.pme.duth.gr/antonis.